Research Article Vol. 57, No. 23 / 10 August 2018 / Applied Optics 6823

applied optics

Optical design of double-grating and double wave band spectrometers using a common CCD

Qingsheng Xue,[1,*] Fengqin Lu,[2] Minzheng Duan,[3,4] Yuquan Zheng,[1] Xiaoheng Wang,[1,4] Diansheng Cao,[1] Guangyu Lin,[1] and Jiewen Tian[1,4]

[1]Changchun Institute of Optics, Fine Mechanics and Physics, Chinese Academy of Sciences, Changchun 130033, China
[2]Changchun UP Optotech (Holding) Co., Ltd, Changchun 130033, China
[3]Institute of Atmospheric Physics, Beijing 130029, China
[4]University of Chinese Academy of Sciences, Beijing 100049, China
*Corresponding author: qshxue2006@163.com

Received 25 May 2018; accepted 16 July 2018; posted 18 July 2018 (Doc. ID 332240); published 10 August 2018

A new type of optical system comprising double-grating and double wave band spectrometers is designed for atmospheric detection. The optical system can bring oxygen A band (758–778 nm) and water vapor absorption band (758–880 nm) on a charge-coupled device (CCD) at the same time for ultrahigh resolution spectrum measurement. Each absorbed band with three observation directions of atmospheric radiation is imaged in different positions of a common CCD. The spectral resolution is less than 0.07 nm in oxygen A band (758–778 nm), and the spectral resolution is less than 0.28 nm in water vapor absorption band (758–880 nm). Three end faces of the optical fiber are on the slit plane for each wave band, and each end face corresponds to an observation angle. The optical fiber core diameter is 600 μm, the slit width is 25 μm, and the slit length is 18.4 mm. The principle of smile correction is analyzed. The smile of the Czerny–Turner double-grating spectrometer can be compensated by using the tilt field lens in front of the focal plane. The design results corroborate that the maximum smile of the double-grating spectrometer is 5 μm and that the approach of correcting smile is effective. The stray light is analyzed, and the approaches of suppressing the stray light are proposed.

OCIS codes: (300.0300) Spectroscopy; (300.6190) Spectrometers; (120.4570) Optical design of instruments; (120.0280) Remote sensing and sensors.

https://doi.org/10.1364/AO.57.006823

1. INTRODUCTION

The Czerny–Turner spectrometer is a commonly used instrument for resolving the spectral intensity of the image across one spatial dimension. Modern designs featuring fixed gratings and a two-dimensional detector have been used for atmospheric sensing [1] and spatially resolved ultrashort pulse measurement [2]. Several applications in remote sensing [3] and ultrashort pulse measurement [4] require a long slit and high spectral resolution over a spectral range. A broadband astigmatism-free Czerny–Turner imaging spectrometer using spherical mirrors [5] was designed by Austin. The length of the slit is 10 mm, and the smile is approximately 50 μm, but the correcting method is not described. The smile must be corrected for the Czerny–Turner spectrometer with a long slit and high spectral resolution.

Here, we affirm that the smile of the Czerny–Turner spectrometer can be corrected using a tilt field lens before the image plane, and the length of the slit is 18.4 mm. We design a double-grating and double wave band spectrometer using a common charge-coupled device (CCD). The main function of the dual-grating spectrometer is to bring the oxygen A band (758–778 nm) and the water vapor absorption band (758–880 nm) on a CCD at the same time for ultrahigh resolution spectrum measurement. Each absorbed band with three observation directions of atmospheric radiation is imaged in different positions of a common CCD. The length of the slit is 18.4 mm. The spectral resolution is less than 0.07 nm in the oxygen A band (758–758 nm), and the spectral resolution of the water vapor absorption band (758–880 nm) is less than 0.28 nm. To suppress the fringe caused by the etalon effect of the CCD detector [6], the angle of the detector in the tangential (dispersive) plane is controlled approximately 0° by using a prism before the image plane.

In Section 2, we describe the sounding principle and design specifications, and in Section 3, we analyze the principle and method of aberration correction. In Section 4, we present a ray tracing and optimization of the double-grating spectrometer and the imaging performance analysis in Section 5.

In Section 6, we present the stray light analysis and suppressing method.

2. SOUNDING PRINCIPLE AND DESIGN SPECIFICATIONS

To improve the comprehensive detection level of the atmosphere, we propose a double-grating and double wave band spectrometer using a common CCD. The oxygen A band (758–778 nm) with three angles and water vapor absorption band (758–880 nm) with three angles can be imaged simultaneously on a common CCD with ultrahigh spectral resolution. The spectrometer is significant for studying the interaction among aerosols, water vapor, and clouds and for accurately assessing the effects of aerosols, water vapor, and clouds on global change, environment, and water cycle. Figure 1 shows the sounding principle. Three telescopes for observation are set for each wave band. The working wave bands of telescopes 1, 2, and 3 are 758–880 nm, and the observing angles are 0°, 15°, 22.5°, respectively. The working wave bands of telescopes 4, 5, and 6 are 758–778 nm, and the observing angles are 0°, 15°, 22.5°, respectively. On the image plane of each telescope, the fiber is used to bring radiation into the entrance slit of the spectrometer. One end face of the fiber is connected to the image plane of the telescope, and the other end face is connected to the entrance slit of the spectrometer. Six end faces of optical fiber are arranged on the entrance slits of the spectrometer. The six end faces of the optical fiber are spectrally imaged on the common CCD detector by the double-grating spectrometer. The six telescopes are on the rotary table and can be used for 2D scanning observation.

Table 1 shows the specifications of the optical system of the double-grating spectrometer.

3. PRINCIPLE AND METHOD OF ABERRATION CORRECTION

A. Spherical Aberration

In the beginning of the design, a spherical mirror's aberrations and Rayleigh criterion are introduced as the design criteria of the relative aperture. The system's F-number is represented as

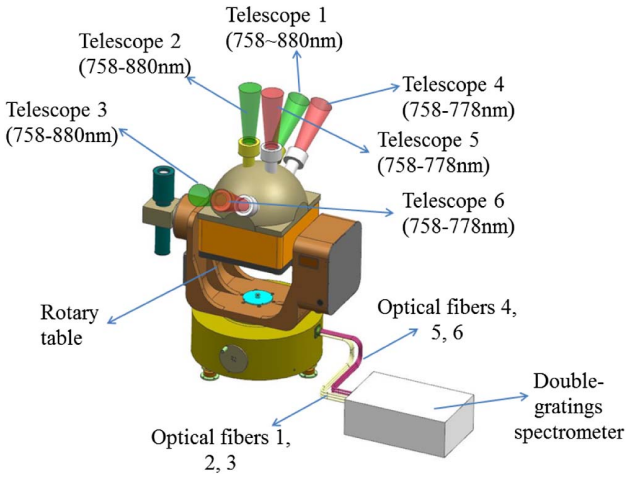

Fig. 1. Diagram of sounding principle.

Table 1. Specifications of the Optical System of the Double-Grating Spectrometer

Spectral range	758–778 nm 758–880 nm
Spectral resolution	0.07 nm 0.28 nm
Field of view of the telescope	1.5°
Diameter of the optical fiber	0.6 mm
Size of the slit	18.4 mm × 0.025 mm
Center coordinates of the slit	(–0.3, 0.5), (0.3, –5.5)
Numerical aperture	0.07
Size of the pixels	11 μm × 11 μm
Size of the CCD detector	2048 × 2048

$F\# = f/D$, where D represents the diameter of the mirror. W is the wavefront aberration due to spherical aberration, as shown in Eq. (1)

$$W_{\max} = \frac{(y_{\max})^4}{8r^3}. \tag{1}$$

According to the Rayleigh criterion, we derive the following equation:

$$\frac{(y_{\max})^4}{8r^3} \le \frac{\lambda}{4}. \tag{2}$$

In Eq. (2), r represents the radius of curvature of the spherical mirror, which equals $2f$, and $y_{\max}$ is the half-aperture of spherical mirror, $D/2$. Equation (2) can be rewritten in the form

$$f \le 256 \cdot \lambda \cdot (F\#)^4. \tag{3}$$

As has been discussed so far, the system's aberration allowance, incident light power, and detecting system should be considered to determine the system's relative aperture.

B. Coma Aberration

A spectrometer based on the asymmetrical Czerny–Turner configuration consists of a grating and collimating and focusing mirrors. Coma aberration was corrected on the basis of the Shafer equation, which is expressed as follows [7,8]:

$$\frac{\sin\alpha_1}{\sin\alpha_2} = \left(\frac{r_1}{r_2}\right)^2 \left(\frac{\cos\theta\cos\alpha_1}{\cos i\cos\alpha_2}\right)^3. \tag{4}$$

Here, α_1 and α_2 are the off-axis incident angle for the central ray on the collimating and imaging mirrors, respectively; i and θ are the incident and diffraction angles on the grating; and r_1, r_2 are the radii of curvature of the collimating and imaging mirrors, respectively. By replacing the third-order terms in α_1 (typically 5°–8°) and α_2 (approximately 10°), as $\cos^3\alpha_1$ and $\cos^3\alpha_1 \cong 1$, we derive the approximate relation,

$$\frac{\sin\alpha_1}{\sin\alpha_2} = \left(\frac{r_1}{r_2}\right)^2 \left(\frac{\cos\theta}{\cos i}\right)^3. \tag{5}$$

Thus, we can eliminate the coma aberration by adjusting the incident α_1, α_2, and curvatures r_1, r_2 to fulfill Eqs. (4) and (5). The spectral profile is asymmetrically deformed by the coma aberration, whereas the spherical aberration symmetrically expands the width. For the Czerny–Turner spectrometer, to make α_1 as small as possible, we set $r_2 > r_1$ based on Eq. (5). We optimize the incident angle to the collimating mirror for a fixed

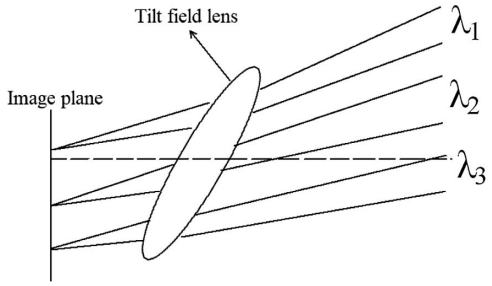

Fig. 2. Schematic diagram of tilt field lens.

imaging mirror, where i and θ are determined by the groove interval and the geometric configuration of the grating based on Eq. (6),

$$d(\sin i + \sin \theta) = m\lambda. \tag{6}$$

Here, d is the groove interval and m is an integer that represents the spectral order.

C. Smile Correction

The two types of dispersion spectrometers are prism and grating. Given that the smile generated by the prism dispersion spectrometer is opposite to the direction of the smile produced by the grating dispersion spectrometer, the two can be deemed complementary.

Several spectrometers use prism gratings for smile correction [9,10]; however, the optical system is highly complicated and can correct only the smile of the center wavelength.

We propose a method of correcting the smile by using a tilting field lens. As the field lens is located near the focal plane, the diffracted beams of different wavelengths are diffracted by the grating converged by the spherical mirror and then are incident on the different positions of the field lens. Therefore, the diffracted beams of different wavelengths pass through small prisms with different thicknesses and top corners at various incident angles. Therefore, different dispersions and smiles will be produced for the diffracted beams of different wavelengths. As the dispersion power of the grating is larger than the dispersion power of the prisms, the grating acts as the main dispersion. The dispersion linearity of the grating spectrometer will not be affected by the dispersion nonlinear of the prism but will have good correction effect on the smile. Figure 2 is a schematic diagram of the tilt field lens. As can be seen from Fig. 2, given that the field lens is close to the image plane, the imaging beams of different wavelengths have been separated, assuming the wavelength from top to bottom $\lambda_1 > \lambda_2 > \lambda_3$.

We analyze several types of a special prism dispersion situation. Figure 3(a) shows that the incident beam is incident from the upper part of the prism, which can simulate the incident situation of wavelength λ_1. Figure 3(b) shows that the incident beam is from the lower part of the prism, which can simulate the incident situation of wavelength λ_3. According to the beam refraction formula and the prism geometry formula, the beam diffraction formulas for the above two cases can be derived as

$$i'_{2a} = \arcsin\{n \sin[\beta + \arcsin(\sin i_1/n)]\}, \tag{7}$$

$$i'_{2b} = \arcsin\{n \sin[\arcsin(\sin i_1/n) - \beta]\}. \tag{8}$$

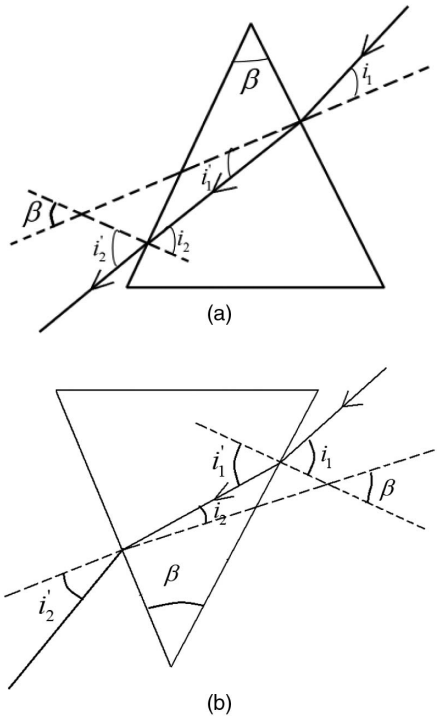

Fig. 3. Several types of a special prism dispersion situation. (a) Incidence from the upper part of the prism. (b) Incidence from the lower part of the prism.

The diffraction angle subscript is distinguished by a and b, respectively, to distinguish between (a) and (b).

For the incident rays at the edge of the slit, the diffraction formula of the component in the main section is similar to the diffraction formula at the midpoint of the slit. Only the refractive index is replaced by N. N is the quantity related to the height of slit, which is called the assumed refractive index

$$N = \sqrt{n^2 + (n^2 - 1)\tan^2 \gamma_1}. \tag{9}$$

In Eq. (9), $\gamma_1 = z/f'$, which is the amount related to the height of the slit. f' represents the focal length of the imaging mirror. The diffraction formulas for the slit edge points are shown in the following equations:

$$\begin{aligned} i'_{2\gamma_a} &= \arcsin\{N \sin[\beta + \arcsin(\sin i_\gamma/N)]\} \\ &= \arcsin\left\{\sin\beta\sqrt{N^2 - \sin^2 i_{1\gamma}} + \cos\beta \sin i_{1\gamma}\right\}, \end{aligned} \tag{10}$$

$$\begin{aligned} i'_{2\gamma_b} &= \arcsin\{N \sin[\arcsin(\sin i_\gamma/N) - \beta]\} \\ &= \arcsin\left\{\sin i_{1\gamma} \cos\beta - \sqrt{N^2 - \sin^2 i_{1\gamma}} \sin\beta\right\}. \end{aligned} \tag{11}$$

In Eqs. (10) and (11), $i_{1\gamma}$ and $i'_{2\gamma}$ are the projections of the incident and diffraction angles, respectively, of the slit-edge ray in the main section and are shown in Fig. 4.

From Eqs. (10) and (11), the amount of smile depends on refractive index N, incident angle i, and the vertex angle of the prism. Therefore, the smile generated by the tilted field lens can

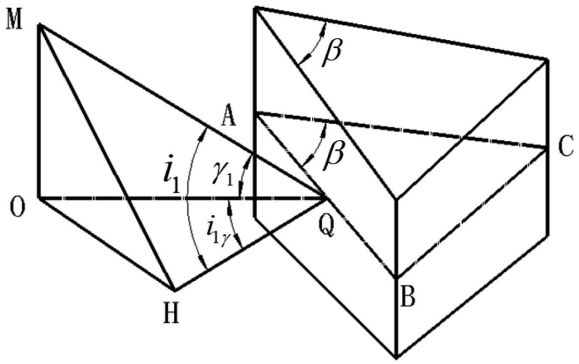

Fig. 4. Incident light projection of the slit edge.

greatly compensate for the smile generated by the grating. Hence, the smile on the imaging focal plane is optimally controlled within a reasonable range.

4. RAY TRACING AND OPTIMIZATION

Ray tracing and optimization design are performed by using ZEMAX [11] software. Figure 5 exhibits the optical fiber input schematic at the entrance slit. The center coordinates of optical fibers 1, 2, and 3 are, respectively, (−0.3, 8.9), (−0.3, 5.5), and (−0.3, 2). The center coordinates of the optical fibers 4, 5, and 6 are (0.3, −2), (0.3, −5.5), and (0.3, −8.9), respectively. The end faces of the optical fibers are connected to the slit, and 3.34 mm away from the slit, a stop is placed. The size of the aperture is matched with the numerical aperture of the spectrometer, and the requirement for suppressing stray light is considered. The spectral range of the light exiting from optical fibers 1, 2, and 3 is 758–880 nm, and the spectral range of the light exiting from optical fibers 4, 5, and 6 is 758–778 nm. Figure 6 illustrates the optical system diagram of the double-grating spectrometer in the X–Z plane (dispersive plane).

Figure 7 depicts the 3D layout of the double-grating spectrometer, as shown in Fig. 7. The rays exiting from the entrance slit are incident on the collimating mirror after passing through the stop. The collimating rays are incident on gratings 1 and 2. The rays in the 758–778 nm band are dispersed by grating 1, and the rays in the 758–880 nm band are dispersed by

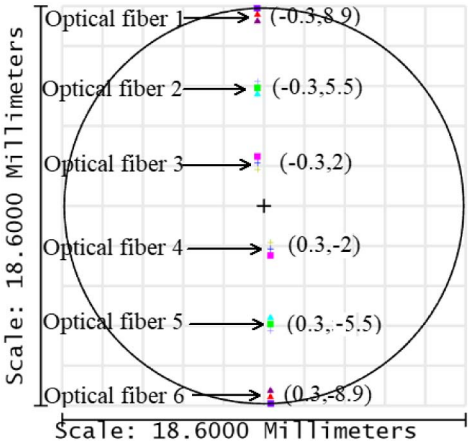

Fig. 5. Optical fiber input schematic at the entrance slit.

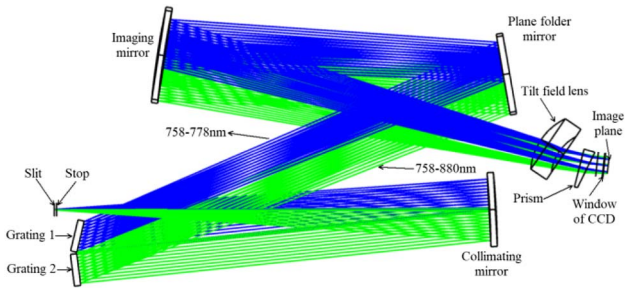

Fig. 6. Optical system diagram of the double-grating spectrometer.

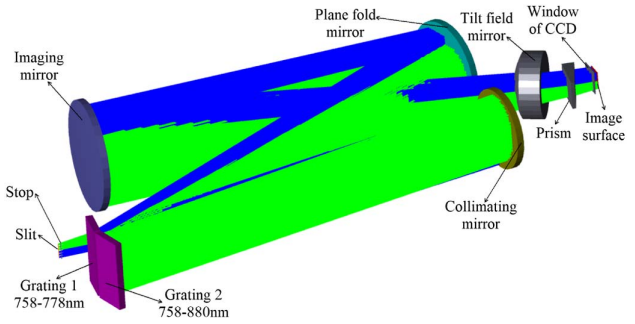

Fig. 7. 3D layout of the double-grating spectrometer.

grating 2. The diffracted rays from gratings are incident on the plane folder mirror. Then, the reflective rays from the plane fold mirror are focused on the image plane by the imaging mirror after correcting the tilt field lens and prism. The collimating and imaging mirrors have spherical surfaces. Figures 8 and 9 show the local enlargement diagram near the entrance slit in the X–Z and Y–Z planes, respectively. Table 2 shows the optical system parameters of the double-grating spectrometer.

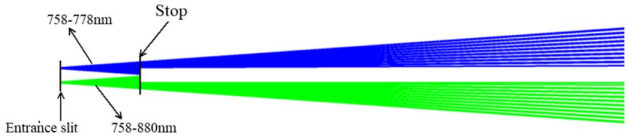

Fig. 8. Local enlargement diagram near the entrance slit in the X–Z plane.

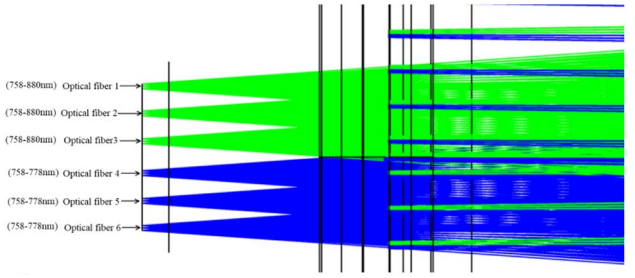

Fig. 9. Local enlargement diagram near the entrance slit in the Y–Z plane.

Figure 10 shows the spectral imager distribution of the six optical fiber end faces on the CCD detector. Figure 11 is an enlarged view of the image plane in the X–Z plane. The images of the six optical fiber end faces are separated from each other in the length direction of the slit, and no spectral aliasing is observed. Under the premise of ensuring no spectral aliasing in the length direction of the slit, the spectral resolution of the spectrometer is increased as much as possible. Therefore, when designing, the imaging quality of the spectrometer in the direction of dispersion is superior to that of the vertical dispersion direction.

Table 2. Optical System Parameters of the Double-Grating Spectrometer

Optical Elements	Thickness (mm)	Radius (mm)	Aperture (mm)
Entrance slit	3.34		7.5 × 0.025
Aperture	554.149		
Collimating mirror	−570	−1196.7	Φ104
Plane grating	634.83		79 × 40(1200 g/mm) 79 × 40(300 g/mm)
Plane fold mirror	−466.53		Φ120
Imaging mirror	530.43	1275.09	Φ140
Tilt field mirror	29.91	83.31	Φ80
	32.09	65.277	Φ56
Prism	10		28 × 28
	22.85		
Window	1		Φ32
	5.41		
Image plane			22.528 × 22.528

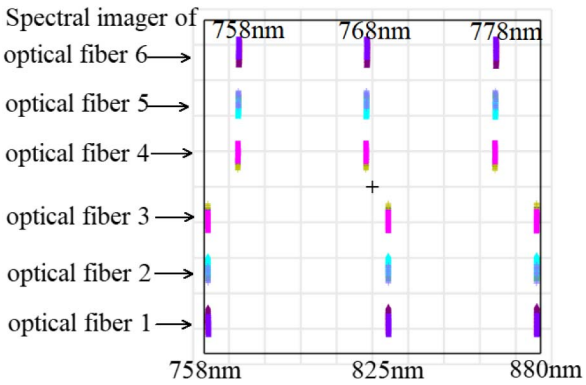

Fig. 10. Spectral imager distribution of the six optical fiber end faces on the CMOS detector.

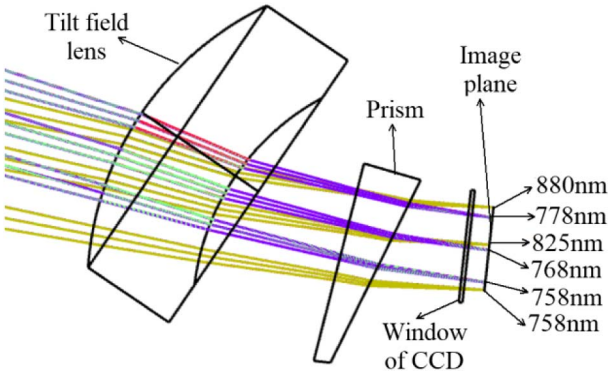

Fig. 11. Enlarged view of the image plane in the X–Z plane.

5. IMAGING PERFORMANCE ANALYSIS

Figures 12 and 13 show the spot diagram on the image plane in 768 nm and 825 nm, respectively. The spot diagram of different wavelengths and fields of view are uniform. The spot diagrams are in rectangle bars, and imaging quality is better in the spectral dimension than in the spatial dimension, which is conducive to obtaining high spectral resolution.

Figures 14(a) and 14(b) exhibit the root meam square (RMS) spot radius versus wavelength in the dispersion direction. The RMS spot diagram radius in dispersion direction is less than 10.29 μm in 758–778 nm band, and the RMS spot diagram radius in dispersion direction is less than 9.68 μm in 758–880 nm

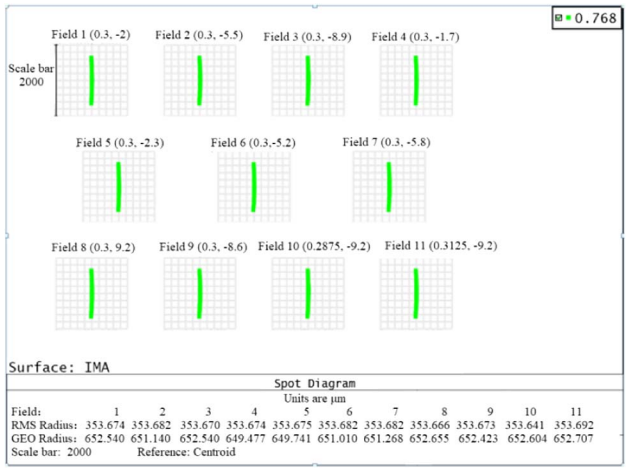

Fig. 12. Spot diagram on image plane in 768 nm.

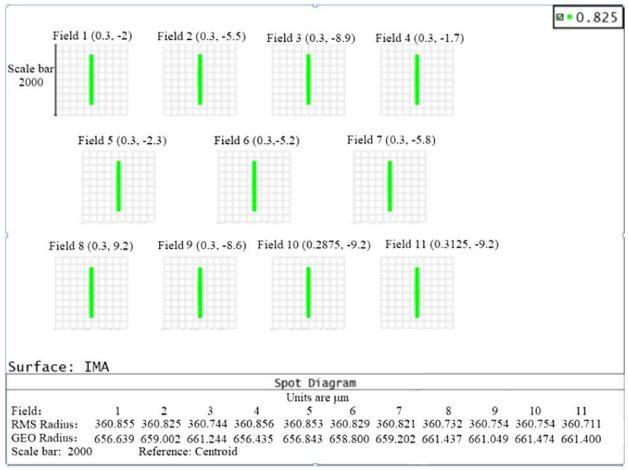

Fig. 13. Spot diagram on image plane in 825 nm.

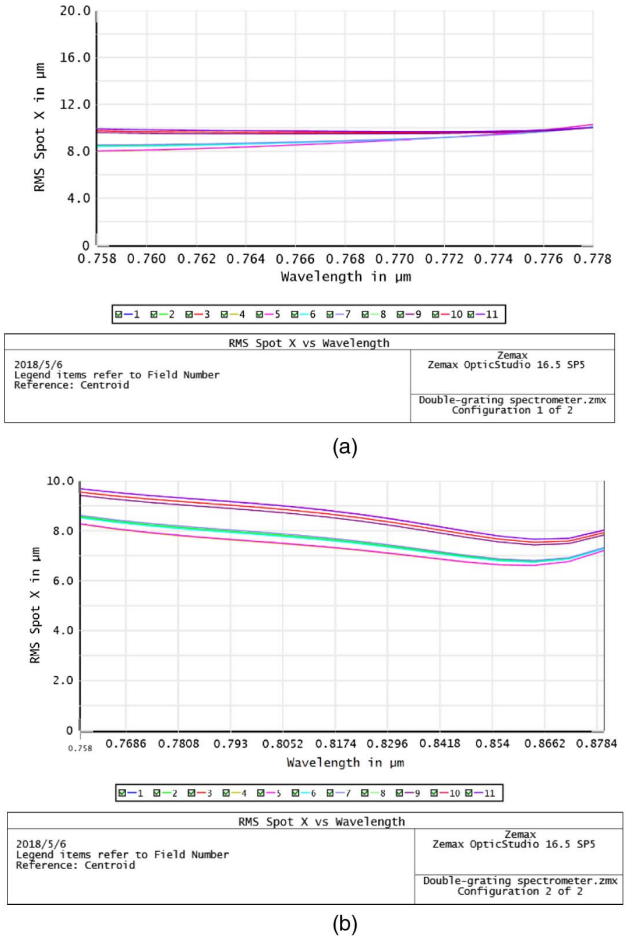

Fig. 14. RMS spot radius versus wavelength in the dispersion direction. (a) 758–778 nm. (b) 758–880 nm.

band. Good imaging quality is obtained at the same time in the wideband. In the 758–778 nm band, the dispersion width on the CCD detector is 17.3272 mm, and the line dispersion rate is $d\lambda_1/dl_1 = 1.154$ nm/mm. In the 758–880 nm band, the dispersion width on the CCD detector is 22.0338 mm, and the line dispersion is $d\lambda_2/dl_2 = 5.5369$ nm/mm.

Table 3 shows the smile for different optical fibers. In the 758–778 nm band, the maximum smile is 5 μm. The maximum smile is 1 μm in the 758–880 nm band. The spectral

Table 3. Smile for Different Optical Fibers

758 nm	Optical fiber 4 1 μm	Optical fiber 5 4 μm	Optical fiber 6 5 μm
768 nm	Optical fiber 4 1 μm	Optical fiber 5 4 μm	Optical fiber 6 5 μm
778 nm	Optical fiber 4 1 μm	Optical fiber 5 3 μm	Optical fiber 6 5 μm
758 nm	Optical fiber 1 0 μm	Optical fiber 2 1 μm	Optical fiber 3 1 μm
825 nm	Optical fiber 1 0 μm	Optical fiber 2 1 μm	Optical fiber 3 1 μm
880 nm	Optical fiber 1 1 μm	Optical fiber 2 1 μm	Optical fiber 3 1 μm

resolution of the two channels is mainly determined by the line dispersion rate, width of the slit image, and the RMS diameters of the spot diagram in the dispersion direction. The spectral resolution in 758–778 nm band can be derived as follows:

$$R_1 = \left(\frac{d\lambda_1}{dl_1}\right) \cdot \sqrt{W_S^2 + W_{D1}^2}. \tag{12}$$

In Eq. (12), $W_s = 0.025$ mm and $W_{D1} = 0.02058$ mm. In the 758–778 nm band, the calculated spectral resolution is 0.0374 nm. By considering bandwidth broadening due to the residual smile, the spectral resolution in the 758–778 nm band is 0.0438 nm, which satisfies the required specification of the spectral resolution of 0.07 nm.

The spectral resolution in 758–880 nm band can be expressed as follows:

$$R_2 = \left(\frac{d\lambda_2}{dl_2}\right) \cdot \sqrt{W_S^2 + W_{D2}^2}. \tag{13}$$

In the formula, $W_S = 0.025$ mm and $W_{D2} = 0.01936$ mm. In the 758–880 nm band, the calculated spectral resolution is 0.1751 nm. By considering bandwidth broadening due to residual smile, the spectral resolution in the 758–880 nm band is 0.1804 nm, which satisfies the required specification of the spectral resolution of 0.28 nm.

6. STRAY LIGHT ANALYSIS AND SUPRESSING METHOD

First, the second-order diffracted light is suppressed by the bandpass filters in the telescope. The out-of-band light is suppressed. The focal length of the telescope is 22.92 mm, field of view is 1.5°, and F number is 2.27. Figure 15 depicts the optical system of the telescope.

Second, to prevent the exiting light from optical fibers 4, 5, and 6 incident on grating 2 while preventing the light exiting from the optical fibers 1, 2, and 3 incident on grating 1, a stop is placed behind the slit. Six transmissive areas are set on the stop, and the rest of the areas are blocked. The distance between the slit and aperture is 3.34 mm. Fibers 4, 5, and 6 (operating band: 758–778 nm) use grating 1 (1200 g/mm), while fibers 1, 2, and 3 (operating band 758–880 nm) use grating 2 (300 g/mm). An optical system model of double-grating spectrometer is established in software Light Tools [12] to analyze the effects of stray light suppression. Figure 16 illustrates the transmissive areas in the stop. The size of each transmissive area is 0.25 mm × 1.04 mm. Figures 17 and 18 depict the simulation results in Light Tools software. Simulation results corroborate that light suppression effect is good. The light exiting from optical fibers 4, 5, and 6 is incident only on grating 1

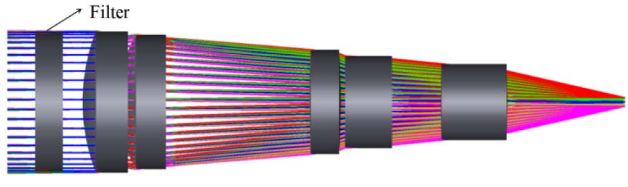

Fig. 15. Optical system of telescope.

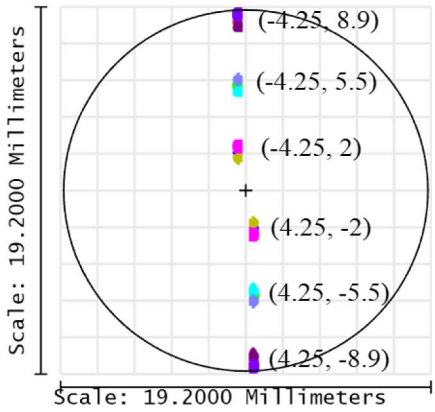

Fig. 16. Transmissive areas in the stop.

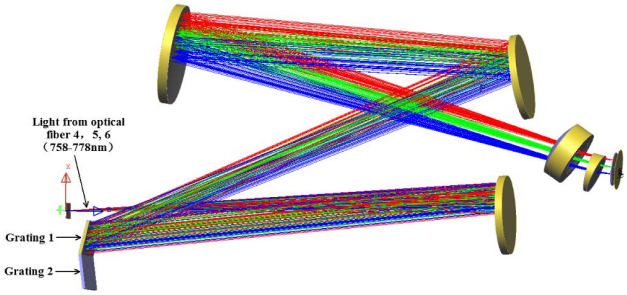

Fig. 17. Optical path diagram for oxygen A band (758–778 nm).

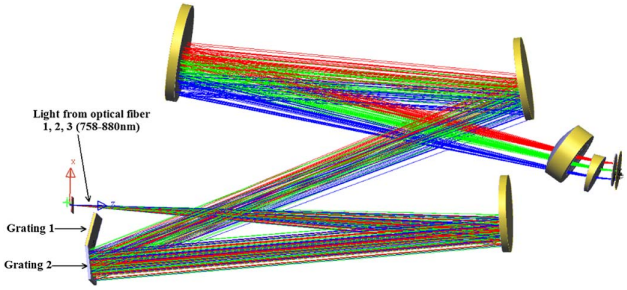

Fig. 18. Optical path diagram for water vapor absorption band (758–880 nm).

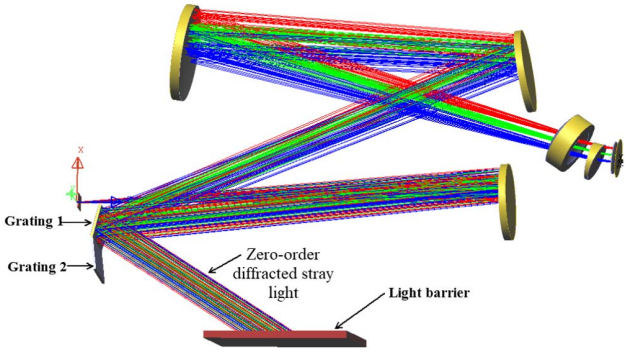

Fig. 19. Zero-order stray light from 758 to 778 nm.

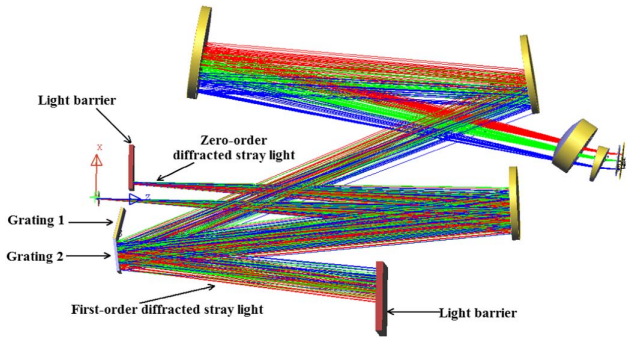

Fig. 20. Zero- and first-order diffracted stray light from 758 to 880 nm.

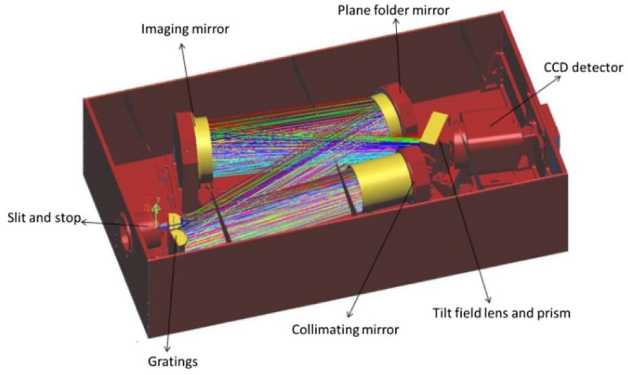

Fig. 21. Optomechanical structure of the double-grating spectrometer.

(1200 g/mm), and the light exiting from optical fibers 1, 2, and 3 is incident only on grating 2 (300 g/mm).

Grating 1 and 2 work at −1 order, while other orders of diffracted stray light are suppressed by setting the light barrier. Figure 19 shows that the zero-order stray light from 758–778 nm is suppressed by a light barrier. Figure 20 shows that the zero-order and first-order diffracted stray light from 758–880 nm is suppressed. Figure 21 is a schematic diagram of an optomechanical structure of the double-gratings spectrometer designed according to the requirements for eliminating stray light.

7. CONCLUSION

A new type of optical system of a double-grating and double wave band spectrometer is designed for atmospheric detection. The optical system can bring oxygen A band (758–758 nm) and water vapor absorption band (758–880 nm) on a CCD at the same time for ultrahigh resolution spectrum measurement. Each absorbed band with three observation directions of atmospheric radiation is imaged on different positions of a common CCD. The spectral resolution is less than 0.07 nm in oxygen A band (758–758 nm), and the spectral resolution is less than 0.28 nm in water vapor absorption band (758–880 nm). We analyze the principle of smile correction in Section 3. The smile of Czerny–Turner double-grating spectrometer can be compensated by using a tilt field lens in front

of the focal plane. The design results validate that the maximum smile of the double-grating spectrometer is 5 μm and prove that the approach of correcting the smile is effective. This approach will be useful for atmospheric imaging, in astronomical imaging, and for studying the structure of ultrashort pulses. On the basis of our analysis, we propose approaches for suppressing stray light.

Funding. National Natural Science Foundation of China (NSFC) (41527806, 41575023); Major Research Plan (2016YFB0500300, 2016YFB0500301, 2016YFB0500302, 2016YFB0500303, 2016YFB0500304).

REFERENCES

1. R. D. Mcpeters, S. J. Janz, E. Hilsenrath, T. L. Brown, D. E. Flittner, and D. F. Heath, "The retrieval of O_3 profiles from limb scatter measurements: results from the Shuttle ozone limb sounding experiment," Geophys. Res. Lett. **27**, 2597–2600 (2000).
2. E. Kosik, A. Radunsky, I. Walmsley, and C. Dorrer, "Interferometric technique for measuring broadband ultrashort pulses at the sampling limit," Opt. Lett. **30**, 326–328 (2005).
3. Q. Xue, "Modified Schwarzschild imaging spectrometer with a low F-number and a long slit," Appl. Opt. **52**, 6956–6961 (2013).
4. A. Wyatt, I. Walmsley, G. Stiblenz, and G. Steinmeyer, "Sub-10 fs pulse characterization using spatially encoded arrangement for spectral phase interferometry for direct electric field reconstruction," Opt. Lett. **31**, 1914–1916 (2006).
5. D. R. Austin, T. Witting, and A. Walmsley, "Broadband astigmatism-free Czerny–Turner imaging spectrometer using spherical mirrors," Appl. Opt. **48**, 3846–3852 (2009).
6. N. Kong, C. Li, M. Xia, Y. Qi, D. Li, and L. Xuan, "Research on flat field correction method in adaptive optics retinal imaging system," Acta Opt. Sin. **31**, 1211001 (2011).
7. A. B. Shafer, L. R. Megill, and L. Droppleman, "Optimization of the Czerny–Turner spectrometer," J. Opt. Soc. Am. **54**, 879–887 (1964).
8. Q. Xue, S. Wang, and F. Lu, "Aberration-corrected Czerny–Turner imaging spectrometer with a wide spectral region," Appl. Opt. **48**, 11–16 (2009).
9. S. Zhu, M. Tang, Y. Ji, G. Gong, and R. Zhang, "Optical design of prism-grating-prism imaging spectrometers," Proc. SPIE **7156**, 7156L01 (2009).
10. M. B. Christiansen, S. Chen, C. S. Baldwin, J. B. Niemczuk, J. S. Kiddy, P. C. Chen, H. K. Kopola, M. Aikio, P. Suopajarvi, and S. G. Buckley, "Digital spatial wavelength domain multiplexing (DSWDM) using a prism-grating-prism (PGP) and a CMOS imager: implementation and initial testing," Proc. SPIE **4328**, 88–95 (2001).
11. ZEMAX, "ZEMAX is a trademark of Zemax Development Corporation," Bellevue, Washington, DC, https://www.zemax.com.
12. "Light tools is a trademark of SYNOPSYS Corporation," https://optics.synopsys.com/lighttools/.